The internal rotation and inversion pathways of the NH 2 group in equatorial amino cyclobutane

ARTICLE *in* JOURNAL OF MOLECULAR STRUCTURE · JULY 2002

Impact Factor: 1.6 · DOI: 10.1016/S0022-2860(02)00145-X

4 AUTHORS, INCLUDING:

Laura B. Favero
Italian National Research Council
84 PUBLICATIONS **866** CITATIONS
SEE PROFILE

Assimo Maris
University of Bologna
97 PUBLICATIONS **946** CITATIONS
SEE PROFILE

ELSEVIER

Journal of Molecular Structure 612 (2002) 357–367

Journal of MOLECULAR STRUCTURE

www.elsevier.com/locate/molstruc

The internal rotation and inversion pathways of the NH_2 group in *equatorial* amino cyclobutane☆

Laura B. Favero[a], Biagio Velino[b], Assimo Maris[c], Walther Caminati[c,*]

[a]*Istituto di Spettroscopia Molecolare del CNR, Via Gobetti 101, I-40129 Bologna, Italy*
[b]*Dipartimento di Chimica Fisica e Inorganica dell'Università, Viale Risorgimento 4, I-40136 Bologna, Italy*
[c]*Dipartimento di Chimica 'G. Ciamician' dell'Università, Via Selmi 2, I-40126 Bologna, Italy*

Received 2 August 2001; accepted 27 September 2001

Abstract

The potential energy surface describing the amino group inversion and internal rotation of *equatorial* amino cyclobutane has been refined, with respect to the results of a previous paper [Chem. Phys. 228 (1998) 219], by using the information obtained from the free jet rotational spectra of the ND_2 and NHD isotopomers and from density functional theory calculations.

The inversion splittings of the ND′H and NH′D (the primed hydrogen lies in the near symmetry plane of the molecule) species (7446.65 and 1062.51 MHz, respectively) were too large to be explained with the above-mentioned model.

Keywords: Rotational spectroscopy; Large amplitude motions; Free jets

1. Introduction

A few years ago, while performing a rather comprehensive investigation of *equatorial–axial* equilibria in mono-substituted cyclobutanes [1–5], we reported the rotational spectrum of amino cyclobutane (ACB) [5]. Besides the *equatorial* and *axial* arrangement of the ring with respect to the substituent, the amino lone electronic pair (LEP) of ACB can be *gauche* or *trans* with respect to the adjacent ring hydrogen. Four stable conformers are expected, labelled as *et*, *eg*, *at* and *ag* (Fig. 1). We could observe only the rotational spectrum of the most stable, the *gauche–equatorial* conformer. Each rotational transition was split into four component lines, due to the four equivalent minima in the two-dimensional (2D) potential energy surface (PES) characterising the inversion and internal rotation of the amino group. We could fit the observed vibrational splittings with a simple 2D model:

$$V(x,y) = (1/2)[V_1\cos(x) + V_3\cos(3x)](y/y_0) + B_0[1-(y/y_0)^2]^2 \quad (1)$$

where x and y describe the internal rotation and the inversion, respectively. y represents the displacement of the dihedral angles HN–CLEP from 90°. $y = 0$ corresponds to the transition state of the inversion, that is to the planarity of the C–NH_2 group, while $y = \pm 30°$ corresponds to the *eg* minima. $x = 0$

☆ This paper is dedicated to Professor Paolo G. Favero and Professor Helmut Dreizler in appreciation of their significant contributions to the field of microwave spectroscopy.

* Corresponding author. Tel.: +39-51-2099-480; fax: +39-51-2099-456.
E-mail address: caminati@ciam.unibo.it (W. Caminati).

0022-2860/02/$ - see front matter
PII: S0022-2860(02)00145-X

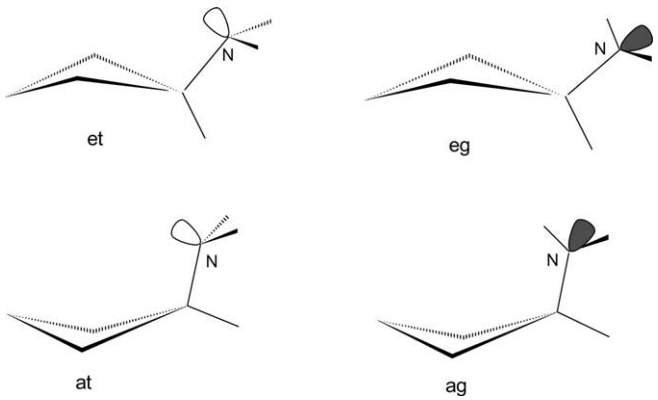

Fig. 1. Drawn of the four *equatorial–axial*, *gauche–trans* conformers of ACB.

represents the *trans* configuration of the LEP when $y<0$, and the *cis* configuration when $y>0$. We assumed $\Delta E(=E_{ct}-E_{eg})=278\ \mathrm{cm}^{-1}$, as suggested by an ab initio investigation [6], and determined $V_1=-370.7\ \mathrm{cm}^{-1}$, $V_3=450.6\ \mathrm{cm}^{-1}$, $B_0=2904\ \mathrm{cm}^{-1}$, and $y_0=33°$.

The amino deuterated and partially deuterated species are expected to be of help in giving more details on the 2D surface. For example, the NH′D and ND′H species (the ′ sign label the hydrogen out of the near symmetry plane NC_1C_4) can have only the inversion motion connecting the two equivalent minima for each isotopomer: the tunnelling due to the internal rotation is quenched because this motion is interconverting the two isotopomers.

For this reason, we decided to investigate these isotopic species. Due to the high spectral density, we made use of a millimetre wave free jet spectrometer, already used to analyse similar problems.

2. Experimental

ACB was purchased from Aldrich and used without further purifications. The microwave measurements have been performed with a free jet spectrometer [7,8]. ACB seeded in argon at a stagnation pressure of ca 30 kPa at room temperature was flown over D_2O for the ND_2 species, and over a mixture of D_2O/H_2O in a ratio 0.55:0.45 for the NHD species, and then expanded to about 50 mPa through a 0.35 mm diameter nozzle.

3. Results and discussion

3.1. Assignment of the rotational spectra

3.1.1. ND_2 species

The assignment of this spectrum was straightforward because (i) the model described in Section 1 was very effective (see later) in calculating the tunnelling splittings of this isotopomer, and (ii) the concentration of the species was almost 100%.

3.1.2. NH′D and ND′H species

The assignments of the rotational spectra were very difficult and needed several sessions at the spectrometer. The reasons were (i) the model used for the normal species did not work at all and produced calculated tunnelling splittings much smaller than the experimental ones; (ii) their concentrations were only 25% in the best conditions, since the NH_2 and ND_2 isotopomers also must be at the same concentration.

The measured transitions are reported in Tables 1 and 2 for the ND_2 and NHD species, respectively. They appear as doublets, due to the inversion splitting. In the case of ND_2 species also the internal rotation should generate a doubling, but it is not resolved with our spectrometer. The hypothetical unsplit central frequencies are given for the lines exhibiting ^{14}N quadrupole hyperfine structure.

The measured transitions of the two sublevels of each isotopomer were fit simultaneously by using Pickett reduced axes system (RAS) [9,10], according

Table 1
Measured frequencies of the ND_2 species of ACB (MHz)

$J(K'_{-1}, K'_{+1})J(K''_{-1}, K''_{+1})$	Interstate transitions		Intrastate transitions	
	01	10	0	1
4(4,1)–3(3,1)			70,951.56[a]	
4(4,0)–3(3,0)			70,948.64[a]	
4(4,1)–3(3,0)	70,388.71	71,508.06		
4(4,0)–3(3,1)	70,392.00	71,511.42		
5(3,3)–4(2,3)			66,096.06[a]	
5(3,3)–4(2,2)	64,671.00	65,783.42		
5(3,2)–4(2,3)	65,630.69	66,743.07		
5(4,2)–4(3,1)	77,418.81			
5(4,1)–4(3,2)	77,441.92			
6(2,4)–5(1,5)	68,809.75	69,924.68		
6(3,4)–5(2,3)	70,997.28	72,115.39		
6(3,3)–5(2,4)	73,202.80	74,320.61		
7(2,6)–6(1,5)	59,780.88	60,895.25		
7(3,5)–6(2,4)	76,881.24	77,964.01		
9(1,9)–8(0,8)		60,228.84		
9(1,8)–8(1,7)			64,034.01	64,033.53
9(2,8)–8(1,7)	69,404.35	70,518.25		
9(2,8)–8(2,7)			62,209.65[a]	
9(2,7)–8(2,6)			66,108.28[a]	
9(3,7)–8(3,6)			63,647.16	63,648.79
9(3,6)–8(3,5)			64,860.17	64,862.29
9(4,6)–8(4,5)			63,773.27	63,774.96
9(4,5)–8(4,4)			63,876.01	63,877.82
9(5,5)–8(5,4)			63,634.62[a]	
9(5,4)–8(5,3)			63,638.38[a]	
9(6)–8(6)[b]			63,539.85[a]	
9(7)–8(7)[b]			63,483.04[a]	
9(8)–8(8)[b]			63,446.54[a]	
10(0,10)–9(0,9)			65,512.75[a]	
10(1,10)–9(1,9)			65,339.72[a]	
10(1,9)–9(1,8)			70,448.07	70,447.40
10(2,9)–9(1,8)	74,219.70			
10(2,9)–9(2,8)			68,848.92[a]	
10(3,8)–9(3,7)			70,659.53	70,660.06
10(4,7)–9(4,6)			70,941.56[a]	
10(4,6)–9(4,5)			71,162.86[a]	
10(5,6)–9(5,5)			70,782.18[a]	
10(5,5)–9(5,4)			70,792.68[a]	
10(6)–9(6)[b]			70,653.95[a]	
10(7)–9(7)[b]			70,575.80[a]	
10(8)–9(8)[b]			70,525.68[a]	
11(0,11)–10(0,10)			71,803.85[a]	
11(0,11)–10(1,10)	70,985.61	72,103.43		
11(1,11)–10(0,10)	71,397.64	72,515.63		
11(1,11)–10(1,10)			71,697.36[a]	
11(1,10)–10(2,9)	71,840.64	72,952.85		
12(0,12)–11(1,11)	77,395.91			
12(1,12)–11(0,11)	77,637.15			
12(1,12)–11(1,11)			78,043.32[a]	

[a] These transitions in the $v = 0$ and $v = 1$ are overlapped to each other.
[b] Doubly overlapped transitions due to the near prolate degeneracy of the involved levels: only K_a is given.

Table 2

Measured transition frequencies of the mono-deuterated species of ACB (MHz)

$J(K'_{-1}, K'_{+1})J(K''_{-1}, K''_{+1})$	ND′H		NH′D	
	10	01	10	01
3(3,0)–2(2,1)	59,814.20			
4(3,2)–3(2,1)	66,927.04		61,095.83	
4(3,1)–3(2,2)	67,297.70		61,472.69	
4(4,1)–3(3,0)	79,237.63	64,354.55	73,786.14	71,662.03
4(4,0)–3(3,1)	79,241.86	64,358.60	73,790.31	71,666.35
5(2,3)–4(1,4)			62,114.04	60,000.90
5(3,3)–4(2,2)	73,850.54		67,963.71	65,789.22
5(3,2)–4(2,3)	74,963.50		69,051.55	66,877.35
5(4,2)–4(3,1)	86,571.10	71,701.30	81,024.80	78,900.50
5(4,1)–4(3,2)	86,600.80	71,731.30	81,054.80	78,930.50
5(5,1)–4(4,0)	98,699.43	83,820.80	93,529.28	91,406.27
5(5,1)–5(4,2)	61,851.72			
5(5,0)–4(4,1)	98,699.43	83,820.80	93,529.28	91,406.27
5(5,0)–5(4,1)	61,849.96			
6(2,5)–5(1,4)	64,027.90			
6(2,4)–5(1,5)			73,239.48	71,124.64
6(3,4)–5(2,3)	80,376.62	65,522.70	74,319.22	72,202.00
6(3,3)–5(2,4)	82,941.20		76,951.48	74,834.83
6(4,3)–5(3,2)	93,852.17	78,997.90	88,212.10	86,087.30
6(4,2)–5(3,3)	93,971.80	79,118.60	88,332.27	86,207.61
6(5,2)–5(4,1)		91,185.00		
6(5,2)–6(4,3)	61,782.56			
6(5,1)–5(4,2)		91,187.00		
6(5,1)–6(4,2)	61,774.04			
6(6)–6(5)	73,951.57			
7(2,6)–6(1,5)			62,536.26	60,421.53
7(3,5)–6(2,4)	86,417.83	71,572.30		78,112.92
7(3,4)–6(2,5)	91,396.40	76,580.00		
7(4,4)–6(3,3)		86,184.20	95,288.48	93,161.56
7(4,3)–6(3,4)		86,546.13	95,648.60	93,521.80
7(5,3)–7(4,4)	61,681.84			
7(5,2)–7(4,3)	61,651.14			
7(6,2)–7(5,3)	73,888.76			
7(6,1)–7(5,2)	73,888.22			
7(7)–7(6)		71,193.30		
8(2,7)–7(1,6)			67,415.09	65,300.70
8(3,6)–7(2,5)		77,111.06		
8(5,4)–8(4,5)	61,546.55			
8(5,3)–8(4,4)	61,456.36			
8(6,3)–8(5,4)	73,798.76			
8(6,2)–8(5,3)	73,796.48			
8(7)–8(6)		71,157.40		
9(0,9)–8(1,8)	68,469.26		61,036.66	
9(1,9)–8(0,8)	69,390.14		62,014.86	
9(1,8)–8(2,7)	67,396.52			
9(2,8)–8(1,7)			72,240.19	70,126.53
9(5,5)–9(4,6)	61,380.62			
9(5,4)–9(4,5)	61,152.53			
9(6,4)–9(5,5)	73,675.62			

(*continued on next page*)

Table 2 (*continued*)

$J(K'_{-1}, K'_{+1})J(K''_{-1}, K''_{+1})$	ND′H		NH′D	
	10	01	10	01
9(6,3)–9(5,4)	73,667.48			
9(7)–9(6)		71,104.60		
10(0,10)–9(1,9)	75,240.10	60,358.59	67,696.90	
10(0,1)–9(1,9)				65,575.93
10(1,10)–9(0,9)	75,781.26	60,898.62	68,275.35	66,154.21
10(1,9)–9(2,8)		60,670.92	67,898.14	
10(2,9)–9(1,8)			77,156.21	75,043.46
10(5,6)–10(4,7)	61,196.41			
10(5,5)–10(4,6)	60,684.75			
11(0,11)–10(1,10)				72,158.33
11(0,11)–10(1,10)			74,278.88	
11(1,11)–10(0,10)			74,614.13	
11(1,11)–10(1,0)				72,493.27
11(5,6)–11(4,7)	59,979.00			

to

$$H = H_R(0) + H_R(1) + H_{CD} + H_{int} \quad (2)$$

where $H_R(0)$ and $H_R(1)$ are related to the rotational energies in the $v = 0$ and $v = 1$ states, H_{CD} account for the centrifugal distortion effects, assumed to be the same for the two sublevels, and H_{int}, the interaction term, is given by

$$H_{int} = \Delta E_{01} + F_{bc}(P_b P_c + P_c P_b) + F_{ab}(P_a P_b + P_b P_a) \quad (3)$$

The spectroscopic constants obtained are listed in Table 3 together with some statistical parameters of the fits.

3.2. Density functional theory calculations

3.2.1. The potential energy surface of the amino group motions of the equatorial conformers

The PES given in Ref. [5] (FCVCF model) does not fit the new experimental data concerning the mono-deuterated species. According to the general philosophy of the scientific investigation, we had to

Table 3
Spectroscopic constants of N-deuterated species of ACB

Species	N–D_2		N–D′H		N–H′D	
Sublevels	0	1	0	1	0	1
A (MHz)	9632.661(8)[a]	9632.631(7)	9730.837(4)	9730.645(6)	9871.237(7)	9871.188(7)
B (MHz)	3862.210(4)	3862.222(5)	4045.604(6)	4045.683(6)	4002.910(5)	4002.936(5)
C (MHz)	3164.940(4)	3165.945(3)	3292.891(4)	3292.926(5)	3233.110(5)	3233.119(5)
Δ_J (kHz)	0.59(2)		0.65(3)		0.60(3)	
Δ_{JK} (kHz)	1.24(2)		1.62(7)		1.5(1)	
Δ_K (kHz)	4.4(3)		4.0(1)		4.5(2)	
δ_J (kHz)	0.067(5)		0.11(2)		0.12(1)	
δ_K (kHz)	1.5[b]		1.5[b]		1.6(4)	
ΔE_{0-1} (MHz)	560.07(3)		7446.66(4)		1062.54(3)	
F_{ab} (MHz)	4.(1)		60.60(1)		3.(1)	
F_{bc} (MHz)	22.87(2)		13.95(2)		24.69(1)	

[a] Errors in parentheses are expressed in units of the last digit.
[b] Fixed at the value of normal species.

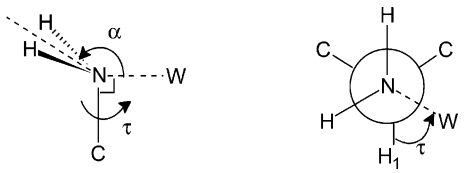

Fig. 2. Definition of the inversion angle α and internal rotation dihedral angle τ. The value of the WNC angle is 90°.

figure out a new model, capable to explain all experimental evidences.

First, in order to have a guide, we explored the 2D PES with a B3LYP/6-31G* calculation. The values of the two leading coordinates (internal rotation τ and inversion α of the amino group, defined in Fig. 2) were fixed at various values in a grid, whereas all the other structural parameters were optimised. The internal rotation coordinate was scanned in the cyclic range $0 < \tau < 360°$ with a step $\Delta\tau = 30°$, while the inversion coordinate was scanned in the range $0 < \alpha < 180°$ with a step $\Delta\alpha = 15°$.

Table 4
Calculated relative electronic energy values (cm^{-1}) of the stationary points of the PES describing the amino group motion in the *equatorial* forms of ACB

	B3LYP/6-311++G**	MP2/6-311++G**
gauche	0	0
trans	312	295
TS_{cis}	1160	1184
TS_{skew}	663	708
TS_{inv}	1137	1586
max	1904	2177

The resulting surface exhibits six kinds of *critical* points: two minima (the *gauche* and *trans* confor-

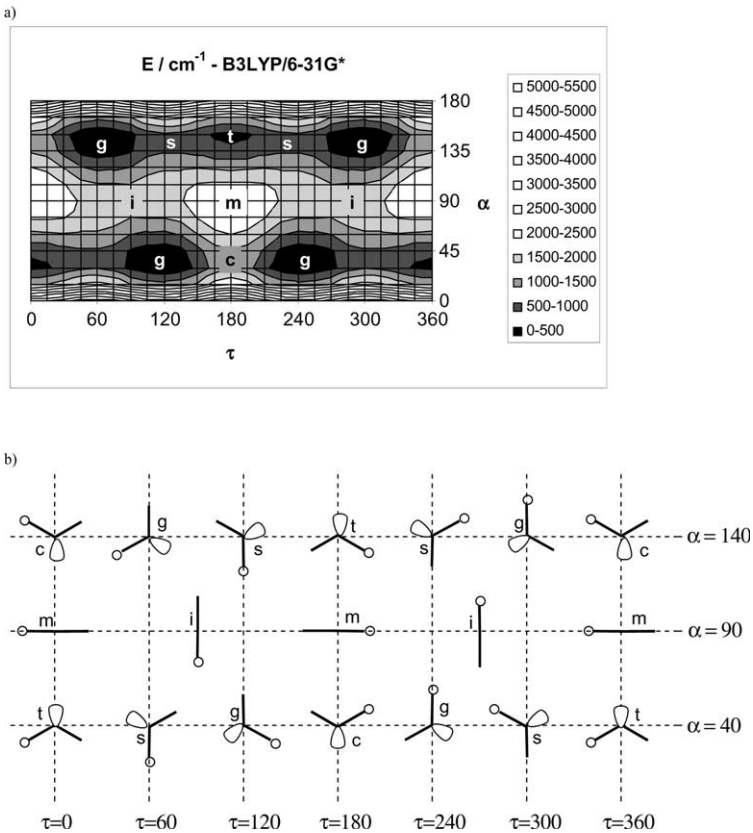

Fig. 3. (a) 2D potential energy function of *eg* ACB (B3LYP/6-31G*). α and τ (Fig. 2) represent the inversion and the internal rotation of the amino group, respectively; (b) rough indication of the position of the amino hydrogens in the stationary points. The labels indicate the lone pair position with respect to H_1, the hydrogen atom attached to C_1. g = *gauche*, t = *trans*, c = *cis*, s = *skew*, $i = TS_{inv}$ and m = max (Section 3.2.1).

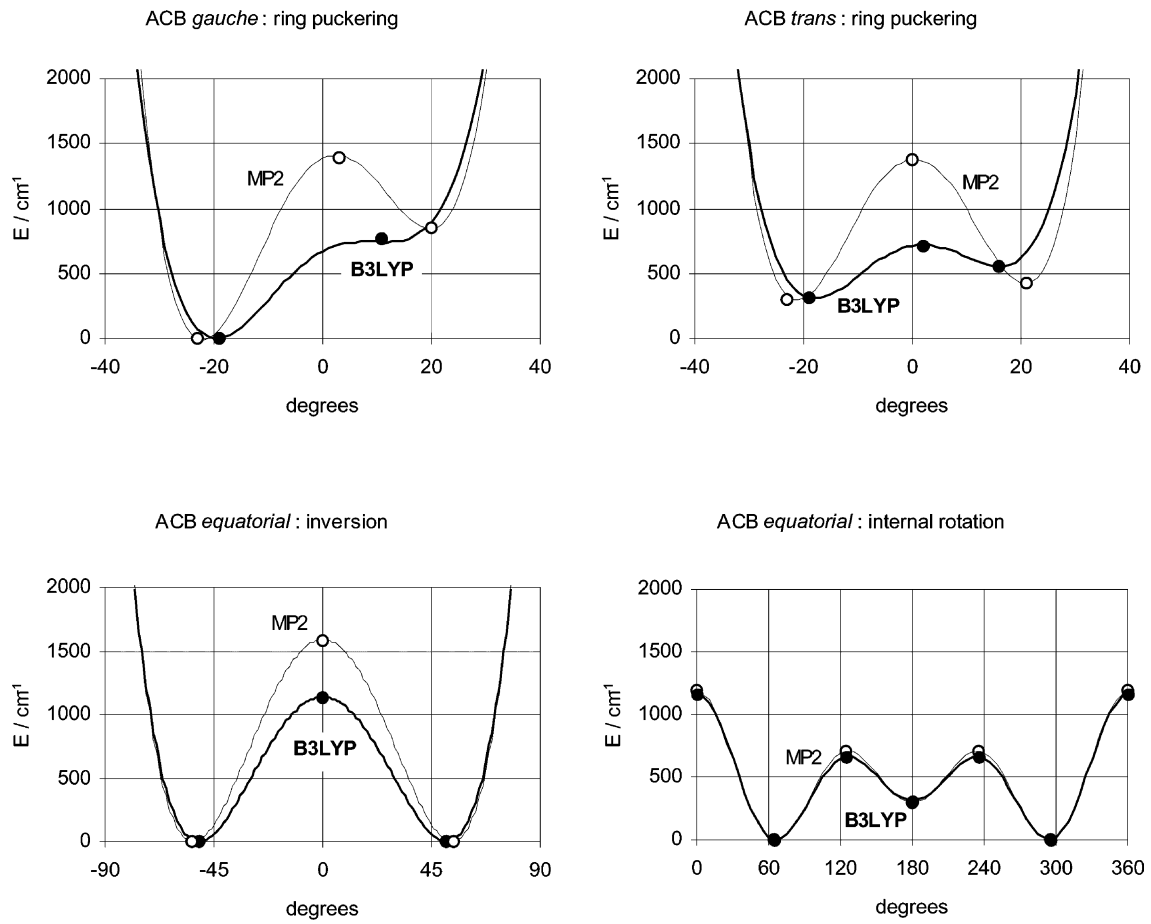

Fig. 4. Potential energy profiles of the large amplitude motions of ACB obtained by the MP2 (empty circles) and the B3LYP (black circles) methods, with a common 6-311++G** basis set.

mers), two transition states due to the NH_2 internal rotation (TS_{cis}, connecting two equivalent minima, and TS_{skew} connecting two different minima), one transition state due to the NH_2 inversion (TS_{inv}), and one global maximum (max).

This 2D PES (Fig. 3) is quite different with respect to that previously reported [5]: a low energy pathway to inversion is now found and the values of the two barriers to internal rotation are higher. Furthermore, the relative height of the two barriers to internal rotation is inverted (now $TS_{cis} > TS_{skew}$).

Improved energy values (Table 4) were then obtained optimising all the structural parameters and employing the 6-311++G** basis set. The saddle points and the maximum were identified by symmetry constrains (TS_{inv}, TS_{cis} and max) or by the automatic transition state optimisation method available in GAUSSIAN98 (TS_{skew}). Finally, a vibrational frequency calculation confirmed definitively the nature of the stationary points: the saddle points show one imaginary frequency, while the maximum shows two imaginary frequencies and the minima do not show any imaginary frequency.

All the quantum chemical computations were performed by the GAUSSIAN98 suite of programs [11].

3.2.2. Conformational equilibrium of ACB

In order to complete the conformational description of ACB, we looked for the *axial* forms and the barriers to the ring-puckering motion. With the same kind of calculations described above, we found the stationary points corresponding to the *axial–trans*

Table 5
Calculated rotational constants, dipole moments and relative electronic energy values of the four conformers of ACB. The ring-puckering barrier (RP) is also reported

	B3LYP/6-311++**				MP2/6-3311++**			
	gauche		*trans*		*gauche*		*trans*	
	Eq	Ax[a]	Eq	Ax	Eq	Ax	Eq	Ax
A (MHz)	9931	–	9924	8409	10,066	8313	10,090	8225
B (MHz)	4188	–	4256	4671	4206	4677	4263	4815
C (MHz)	3352	–	3365	3860	3381	3962	3387	4052
μ_a (D)	0.36	–	−0.26	0.59	0.48	−0.79	−0.21	0.68
μ_b (D)	−1.13	–	0	0	−1.22	1.13	0	0
μ_c (D)	0.30	–	−1.27	−1.09	0.36	0.25	−1.36	−1.15
$\lvert\mu_{tot}\rvert$ (D)	1.22	–	1.29	1.25	1.35	1.40	1.38	1.34
E (cm^{-1})	0[b]	–	312	557	0[c]	856	295	423
RP barrier (cm^{-1})	–		712		1386		1378	

[a] Not a stationary point.
[b] Electronic energy = −212.628490 Hartrees.
[c] Electronic energy = −211.965741 Hartrees.

conformer and to the ring-puckering barrier, but it was not possible to localise the *axial–gauche* conformer. We cannot, however, exclude an energy minimum for the *axial–gauche* conformer, because by using MP2/6-311++G** method we succeeded in localising this species. The comparison between the energy profiles of the internal motions obtained with the two methods (MP2 and B3LYP, common 6-311++G** basis set) is shown graphically in Fig. 4. The results obtained with the two kinds of calculations are similar for the amino group internal rotation, while their difference increases in going to the amino group inversion and to the ring puckering. In Table 4 we give the MP2 energy values of the stationary points of the PES describing the amino group motions in the *equatorial* forms.

In Table 5 we report the rotational constants, the dipole moments and the relative electronic energies obtained with the two methods (MP2 and B3LYP) for the four conformers.

3.3. Potential energy surface for amino group large amplitude motions

The DFT calculations showed that the pathway to inversions has a much lower potential energy profile than that of inversion in ammonia, considering the combination of the inversion and internal rotation. Furthermore, the potential energy profile of the amino group internal rotation takes place at much higher energy than that suggested in Ref. [6]. In our first model (FCVCF model), based on these two considerations, we assumed the barrier to inversion to be higher than the barrier to internal rotation. However, we assume the contrary, by judging the experimental evidences and guided by the DFT calculations. The interpretation of the experimental observations of the internal rotation and inversion of the amino group is given with 1D and 2D flexible model approaches [12]. This model allows the calculation of the energies and wave functions related to two simultaneous motions. Structural relaxations can be taken in consideration as a function of the leading coordinates.

3.3.1. 1D amino group inversion

As previously outlined the tunnelling splittings observed in the rotational spectra of the NH′D and ND′H species must exclusively be due to the inversion because the internal rotation connects two different isotopomers. As a consequence the two (NH′D and ND′H) inversion splittings can be used to determine the barrier to inversion of the H (or D) out of the near symmetry plane of ACB.

We used the following expression for the inversion

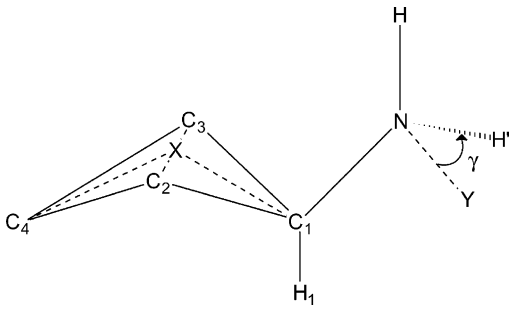

Fig. 5. Drawn of the *equatorial–gauche* conformer of ACB. The dummy atom X and the inversion parameter γ, used in the 1D analysis of the amino group inversion, are indicated. The γ dummy lies in the NC_1H_1 plane

potential:

$$V(\gamma) = B_0[1 - (\gamma/\gamma_0)^2]^2 \quad (4)$$

where γ, the angle H′NY, represents the inversion motion of the H′ (or D′) atom, and it is 0 when H′ is coplanar to H_1. B_0 is the barrier to inversion and γ_0 is its equilibrium value. We had to use a different coordinate, with respect to the 2D model, to describe the inversion of a single hydrogen atom. γ is shown in Fig. 5, where the labelling of atoms and the definition of the 'dummy' atoms X and Y are also given. The following structural relaxations, as suggested by the DFT calculations, were also included in the model:

$$r(\mathrm{CN}) = 1.4288 + 0.0216(\gamma/\gamma_0)^2 \quad (5)$$

$$r(\mathrm{NH}) = 1.0030 + 0.0120(\gamma/\gamma_0)^2 \quad (6)$$

$$r(\mathrm{C_1X}) = 1.1228 - 0.0061(\gamma/\gamma_0)^2 \quad (7)$$

$$r(\mathrm{C_2X}) = 1.0839 + 0.0120(\gamma/\gamma_0) \quad (8)$$

$$r(\mathrm{C_3X}) = 1.0839 - 0.0120(\gamma/\gamma_0) \quad (9)$$

$$\angle(\mathrm{HN{-}C_1H_1}) = 180.0 - 4.8(\gamma/\gamma_0) \quad (10)$$

$$\angle(\mathrm{NC_1{-}XC_2}) = -90.0 - 5.0(\gamma/\gamma_0) \quad (11)$$

$$\angle(\mathrm{YN{-}C_1H_1}) = 0.0 - R_\gamma(\gamma/\gamma_0) \quad (12)$$

This last equation takes account of the coupling, within the 1D model, of the inversion with the internal rotation. B_0 and R_γ, which represents the relaxation of $\mathrm{YN{-}C_1H_1}$ as a function of γ, have been estimated from the two splittings, while γ_0 and the other structural relaxation parameters have been fixed to the DFT values. The 1D Meyer's flexible model has been used [12]. Six vibrational states were calculated on a grid of 43 mesh points in the range $-100 \leq \gamma \leq 100°$ for each isotopomer. Table 6 shows these data, together with the experimental and calculated values of the four inversion splittings. One can see that although the NH_2 and ND_2 species require a more complicated model (since the two motions connect four equivalent minima), the calculated splittings qualitatively reproduce the experimental values.

In agreement with the DFT calculations, the inversion barrier becomes much lower when combined with the amino group internal rotation, than the value for ammonia, where a motion such as the internal rotation is not possible.

Table 6
1D flexible model results for the amino group inversion in *eg* ACB (see Section 3.3.1 and Eqs. (4)–(12))

Flexible model parameters		
B_0 (cm^{-1})	886.4	
γ_0 (°)	54.4[a]	
R_γ	6.04	
Vibrational spacings (MHz)		
Species	ΔE_{01}	
	Obs.	Calc.
ND′H	7446.66(4)[b]	7446.3
NH′D	1062.54(3)[b]	1062.3
NH_2	11,874.15(3)	12,986.7
ND_2	560.07(3)	703.4

[a] Fixed at the DFT value.
[b] Used to determine B_0 and R_γ.

3.3.2. 1D amino group internal rotation

Only one splitting due to the internal rotation for the normal species is available (7.98 MHz). The splitting of the ND_2 species is too small to be detected with our spectrometer. The DFT potential energy profile could be satisfactorily represented by the following function:

$$V(x) = 468 - 70\cos(x) + 233\cos(2x) - 354\cos(3x) + 36\cos(4x) \quad (13)$$

Our experimental splitting could be reproduced by

Table 7
2D flexible model results for the amino group inversion and internal rotation in *eg* ACB (see Section 3.3.3 and Eq. (14))

Flexible model parameters (slightly different with respect to the DFT values: adapted to better reproduce the observed splittings)			
B_0 (cm^{-1})	886[a]		
γ_0 (°)	31.5		
C	0.4		
F	0.70		
R_{xy}	−5.0		
Vibrational spacings (MHz)			
Motion	Species	ΔE_{01}	
		Obs.	Calc.
Inversion	ND′H	7446.66(4)	6259.0
	NH′D	1062.54(3)	954.2
	NH_2	11,874.15(3)	11,947.1
	ND_2	560.07(3)	499.1
Internal rotation	NH_2	7.95(5)	8.3
	ND_2	<0.3	0.1

[a] This is not exactly the barrier to inversion, whose value, 856 cm^{-1}, can be obtained from Eq. (14).

scaling this function to a factor 1.03. The same flexible model described above was used. We did not include, this time, structural relaxation because they did not appear very large, and also because they were difficult to be expressed by simple functions of x.

3.3.3. 2D model

We tried, finally, to interpret all the observed splittings treating simultaneously the two motions. The following function, appropriate for the symmetry properties of our problem, has been used to describe the 2D PES:

$$V(x,y) = (1/2)F\{[V_1\cos(x) + V_3\cos(3x)](y/y_0) + [V_2\cos(2x) + V_4\cos(4x)](y/y_0)^2\} + B_0[1 + C\cos(2x)](1 - (y/y_0)^2)^2 \quad (14)$$

where x and y, which describe the internal rotation and the inversion, respectively, are the same parameters used in Ref. [5] and already described in Section 1. The parameter F represents a scale factor for the DFT potential energy function to internal rotation, while C is a factor of the modulation (guided by the parameter x and suggested by the DFT calculations) of the barrier to inversion. The parameter F of Eq. (14) was adapted to reproduce the NH_2 internal rotation splitting. The other parameters were fixed to the 1D value (B_0) or to the DFT values (the remaining ones). All structural relaxations of Eqs. (5)–(12) were included in the calculation, but Eq. (11) needed, because of the symmetry of the problem, to be rewritten as

$$\angle(NC_1{-}XC_2) = -90.0 + R_{xy}\{0.38[1 - \cos(2x)](y/y_0) - 1/4[\cos(3x) - \cos(x)][(y/y_0)^2]\mathrm{sgn}[\sin(x)]\} \quad (15)$$

R_{xy} represents the relaxation of $NC_1{-}XC_2$, which is now a function of both x and y (sgn is the function 'sign of'). The scale factor F (0.7) can probably account for the remaining structural relaxation associated to x, which have not been included in the calculations. Twenty vibrational states were calculated on a grid of 61 mesh points in the range 2π for x, times 41 mesh points in the range $-60 \le y \le 60°$ [12]. The results of the 2D flexible model calculations are shown in Table 7.

4. Conclusions

The DFT calculations and the rotational spectra of the NH′D and ND′H species unambiguously show that the barrier to inversion in ACB is much smaller than the value previously reported and than in the case of the prototype molecule ammonia. The combination with the amino group internal rotation generates low energy pathways to inversion, as shown in Fig. 3.

The DFT calculations resulted as a good guiding tool in exploring complex PESs due to large amplitude motions such as for ACB.

The failure in observing other conformers besides the *eg* one is somehow explained by the DFT calculations, which suggests very small holes for the other conformers, where it is difficult to locate stable vibrational states.

Acknowledgments

We are grateful to Mr A. Millemaggi for technical help. The University of Bologna, the Ministero dell'Università e della Ricerca Scientifica e Tecnologica, and the Consiglio Nazionale delle Ricerche are aknowledged for financial support.

References

[1] W. Caminati, B. Velino, M. Dakkouri, L. Schäfer, K. Siam, J.D. Ewbank, J. Mol. Spectrosc. 123 (1987) 469.
[2] W. Caminati, B. Velino, R.G. Della Valle, J. Mol. Spectrosc. 129 (1988) 284.
[3] W. Caminati, L.B. Favero, A. Maris, P.G. Favero, J. Mol. Struct. 376 (1996) 25.
[4] B. Velino, L.B. Favero, W. Caminati, J. Mol. Spectrosc. 179 (1996) 168.
[5] L.B. Favero, G. Corbelli, B. Velino, W. Caminati, P.G. Favero, Chem. Phys. 228 (1998) 219.
[6] T. Jonvik, J.E. Boggs, J. Mol. Struct. 105 (1983) 201.
[7] S. Melandri, W. Caminati, L.B. Favero, A. Millemaggi, P.G. Favero, J. Mol. Struct. 352/353 (1995) 253.
[8] S. Melandri, G. Maccaferri, A. Maris, A. Millemaggi, W. Caminati, P.G. Favero, Chem. Phys. Lett. 261 (1996) 267.
[9] H.M. Pickett, J. Chem. Phys. 56 (1972) 1715.
[10] H.M. Pickett, J. Mol. Spectrosc. 148 (1991) 371.
[11] M.J. Frisch, G.W. Trucks, H.B. Schlegel, G.E. Scuseria, M.A. Robb, J.R. Cheeseman, V.G. Zakrzewski, J.A. Montgomery Jr., R.E. Stratmann, J.C. Burant, S. Dapprich, J.M. Millam, A.D. Daniels, K.N. Kudin, M.C. Strain, O. Farkas, J. Tomasi, V. Barone, M. Cossi, R. Cammi, B. Mennucci, C. Pomelli, C. Adamo, S. Clifford, J. Ochterski, G.A. Petersson, P.Y. Ayala, Q. Cui, K. Morokuma, D.K. Malick, A.D. Rabuck, K. Raghavachari, J.B. Foresman, J. Cioslowski, J.V. Ortiz, A.G. Baboul, B.B. Stefanov, G. Liu, A. Liashenko, P. Piskorz, I. Komaromi, R. Gomperts, R.L. Martin, D.J. Fox, T. Keith, M.A. Al-Laham, C.Y. Peng, A. Nanayakkara, C. Gonzalez, M. Challacombe, P.M.W. Gill, B. Johnson, W. Chen, M.W. Wong, J.L. Andres, C. Gonzalez, M. Head-Gordon, E.S. Replogle, J.A. Pople, GAUSSIAN98, Revision A.7, Gaussian, Inc., Pittsburgh, PA, 1998.
[12] R. Meyer, J. Mol. Spectrosc. 76 (1979) 266.